Comparison of observed and calculated shapes of travelling cavitation bubbles

Y.Kuhn de Chizelle and C.E.Brennen
California Institute of Technology

Abstract. Recent observations of the geometries of growing and collapsing bubbles in typical cavitating flows (van der Meulen and van Renesse 1989, Briancon-Marjollet and Franc 1990, Ceccio and Brennen 1991, Kuhn de Chizelle *et al.* 1992) have revealed the complexity of the "microfluidmechanics" associated with these flows. Clearly the interaction of individual bubbles with the nearby solid surface and its boundary layer produce features in the dynamics of growth and collapse which were not present in experiments on bubbles in a quiescent liquid. These include several mechanisms for bubble fission prior to collapse and the role played by the concentration of accumulated vorticity in producing a hybrid vortex/bubble during collapse.

The current paper presents a methodology for the calculation of the interaction between an individual bubble and the irrotational flow exterior to the boundary layer on a body. Comparison is made between computed bubble geometries and those previously observed experimentally. The calculations also reveal the effect which the bubble has on the irrotational flow around the body and consequently permits some preliminary evaluation of the interactions between neighbouring bubbles.

Key words: Cavitation, Bubble, Travelling, Flow, Interactions, Computation

1 Introduction

The focus of this paper is on travelling bubble cavitation and the interactions between the flow and the bubbles which can occur in this type of cavitating flow. It is motivated by the fact that these interactions radically alter the dynamics of bubble collapse and therefore the noise and damage potential of that process.

The dynamics of collapsing cavitation bubbles have received much attention since it was first recognized that the violence of the collapse was responsible for cavitation damage. The mechanisms of shock wave production during rebound (Gilmore 1952, Hickling and Plesset 1964) and reentrant microjet shocks (Naude and Ellis 1961, Benjamin and Ellis 1966, Lauterborn and Bolle 1975, Fujikawa and Akamatsu 1980, Shima *et al.* 1981 & 1983, Kimoto 1987) have been extensively explored both experimentally and analytically. Yet virtually all of these observations and analyses have focused on bubble collapse in a quiescent liquid despite the fact that a number of experimenters have commented on the deformation of cavitation bubbles by the flow (see, for example, Knapp and Hollander 1948, Parkin 1952, Ellis 1952, Blake *et al.* 1977). Until the recent work of van der Meulen and van Renesse (1989), Briancon-Marjollet and Franc (1990), Ceccio and Brennen (1991), Kumar and Brennen (1991, 1992) and Kuhn de Chizelle *et al.* (1992), the nature and consequences of this deformation had not been examined. It is now clear that the deformation and fission caused by the interaction of the bubble with the nearby solid surface and with the pressure gradients and shear in the flow play a very im-

J. R. Blake et al. (eds.), Bubble Dynamics and Interface Phenomena, 207–217.

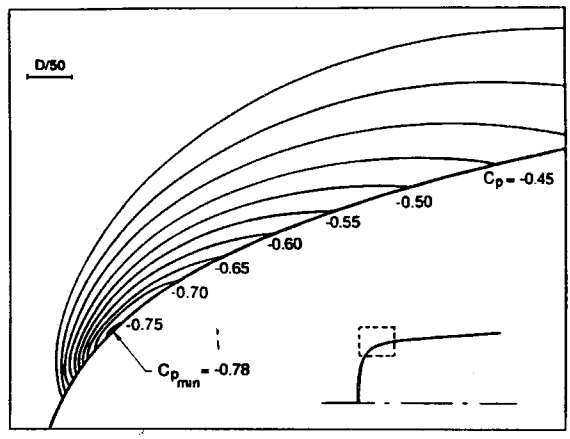

Fig. 1. Isobars in the vicinity of the minimum pressure point on the axisymmetric Schiebe headform with values of the pressure coefficient, C_p, as indicated. The pressures were obtained from a potential flow calculation. The insert shows the headform shape and the area that has been enlarged in the main figure (dashed lines).

portant role in the dynamics and acoustics of travelling bubble cavitation. This paper presents the results of one effort to model some aspects of that interaction.

The papers by van der Meulen and van Renesse (1989), Ceccio and Brennen (1991) and Kuhn de Chizelle *et al.* (1992) constitute an extended series of observations of travelling cavitation bubbles in the flow around axisymmetric headforms and reveal a rich complexity in the "microfluidmechanics" associated with the interactions between the bubbles, the solid surface and the flow. The experiments of Ceccio and Brennen and of Kuhn de Chizelle *et al.* utilized axisymmetric headforms typified by the "Schiebe" body whose approximate shape is shown in figure 1 along with the details of the isobars in the low pressure region according to a potential flow analysis. The coefficient of pressure, C_p, is defined in the usual way as $C_p = 2(p - p_\infty)/\rho U^2$ where U is the tunnel velocity, ρ the liquid density, and p_∞ and p are respectively the tunnel pressure and the local pressure. Note the large pressure gradient normal to the surface in the vicinity of the minimum pressure point which contributes to the bubble deformation.

Typical photographs of bubbles during the growth and collapse cycle are shown in figure 2 taken from Ceccio and Brennen (1991); they are all for the same cavitation number, σ, defined in the usual way as $\sigma = 2(p_\infty - p_v)/\rho U^2$ where p_v is the vapor pressure. For most of its cycle, the bubble has approximately a spherical cap shape, the bubble being separated from the headform surface by a thin layer of liquid which is of the same order of magnitude as the boundary layer thickness. As the bubble begins to enter the region of adverse pressure gradient the outer front surface begins to be pushed inward causing the profile of the bubble to appear wedge-like. Thus the collapse is initiated on this outer front surface of the

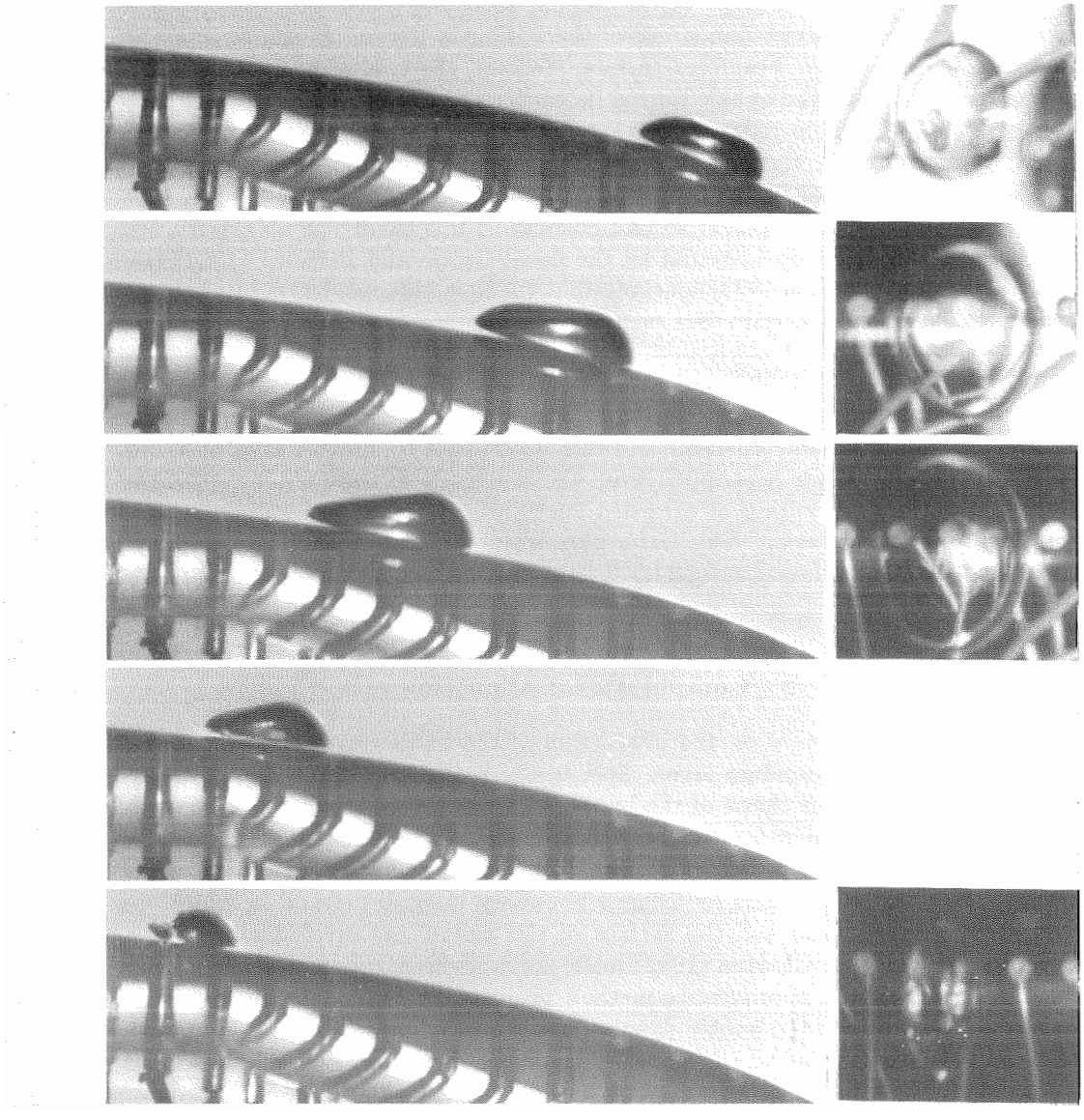

Fig. 2. A series of photographs illustrating the growth and collapse of travelling cavitation bubbles in a flow around a 5.08 cm diameter Schiebe headform at $\sigma = 0.45$ and a speed of 9 m/s. Tunnel blockage effects imply an effective $\sigma = 0.40$. Simultaneous profile and plan views are presented but each row is, in fact, a different bubble. The flow is from right to left and the scale is 4.5 times lifesize. From Ceccio and Brennen (1991).

bubble and this often leads to the bubble fissioning prior to collapse (as seen in the third row of figure 2). Two other processes are occurring at the same time. First, the streamwise thickness of the bubble decreases faster than its spanwise breadth so that the major dimension of the bubble is normal to the direction of flow and parallel to the headform surface. Second, the spanwise vorticity which has been acquired by the bubble during its earlier growth phase is now being concentrated as the bubble collapses so that the bubble evolves into one or two (or possibly more) hybrid vortex/bubbles with spanwise axes. These vortex/bubbles proceed to collapse and seem to rebound as a cloud of much smaller bubbles (last row, figure 2). Often a coherent second collapse of this cloud was observed when the bubbles were not too scattered by the flow. Ceccio and Brennen (1991) (see also Kumar and Brennen 1993) conclude that the flow-induced fission prior to collapse can have a substantial effect on the noise impulse produced by this kind of cavitation event.

Ceccio and Brennen (1991) and Kuhn de Chizelle *et al.* (1992) observed several other important interaction phenomena. Sometimes the thin liquid layer under the bubble would become unstable and this would lead to another kind of fission in which a bubbly layer is stripped from the underside of the bubble. Also, the bubble can trigger a region of attached cavitation in its wake as it passes the minimum pressure location. This latter phenomenon becomes much commoner as the Reynolds number increases and leads to important scaling effects on cavitation noise.

2 Computational Algorithm

The present paper focuses on the interaction of the bubble with the irrotational flow exterior to the boundary layer. Specifically it is directed toward an understanding of the exterior shape of the bubble. Clearly, other viscous flow analyses are needed in order to understand the phenomena of the liquid layer instability and the triggering of attached cavitation. It is, of course, possible to solve the inviscid, irrotational problem by using a boundary integral method in which the surface of the headform and the surface of the bubble are divided into boundary elements. Indeed, Chahine (1992) made some preliminary calculations of this kind. We believe the approximate method presented here has the advantage of improved resolution of the bubble dynamics at much reduced computational time. It could also be extended to allow studies involving more than one bubble so that interaction effects might be examined.

One of the basic, simplifying assumptions behind the current model is that the perturbations in the irrotational flow caused by the bubble can be fairly accurately modelled by a simple travelling source of adjustable intensity and position and that, once an image source is added to substantially satisfy the boundary condition on the headform surface, the remaining corrections which are required involve small modifications of the basic structure of the flow. Only a brief account of the model

will be given here; for further details the reader is referred to Kuhn de Chizelle (1993). In brief, the numerical model combines the following elements:

1. The oncoming uniform stream of velocity, U, whose velocity potential at a point, C, in the fluid whose cylindrical coordinates are (r_c, x_c) is Ux_c.

2. A series ($i = 1$ to N_p) of axisymmetric ring panels of normalized strength, μ_i, and radius, r_{pi}, on the surface of the headform (diameter, D). The axial coordinates of the end points of each panel are denoted by x_i and x_{i+1}. The induced velocity potential, ϕ_{pi}, due to one of these ring panels at a point, C, in the fluid whose cylindrical coordinates are (r_c, x_c) is (Kellogg 1953)

$$\phi_{pi} = \mu_i A_i(r_c, x_c) \; ; \; A_i = \int_{x_i}^{x_{i+1}} \int_0^{\pi} \frac{2 \, d\theta \, dx}{\{r_c^2 + r_{pi}^2 + (x_c - x)^2 - 2 r_c r_{pi} cos\theta\}^{\frac{1}{2}}} \quad (1)$$

   The present calculations used 93 rings with a special concentration in the low pressure region.

3. A point source of time-varying intensity, $q(t)$, placed at some chosen location, (r_q, x_q), in the $\theta = 0$ plane of symmetry. This source, which is used to simulate the bubble, induces a velocity potential, ϕ_q, at any point, C, where

$$\phi_q = qA_q(r_c, \theta_c, x_c) = -q/4\pi d_{qc} \quad (2)$$

   where d_{qc} is the distance between the source and the point C.

4. An image source of identical strength placed inside the headform at the image point which is equidistant from the headform surface. The line joining the source and its image must be a normal to the headform surface. The potential due to this image is denoted by $\phi_{\bar{q}} = qA_{\bar{q}}(r_c, \theta_c, x_c)$.

Then the combined velocity potential for the entire flow, ϕ, is given by

$$\phi(r_c, \theta_c, x_c) = Ux_c + \sum_{i=1}^{N_p} \mu_i A_i(r_c, x_c) + qA_q(r_c, \theta_c, x_c) + qA_{\bar{q}}(r_c, \theta_c, x_c) \quad (3)$$

and, provided q, r_q and x_q are known, the entire flow field can be solved by conventional means by using the condition that the normal velocity be zero in the center of each of the N_p ring panels. These N_p conditions determine the N_p unknowns, μ_i, $i = 1$ to N_p. In the current program a standard orthogonalization procedure was used for this purpose.

The program begins when a stable nucleus of specified size, R_0, is introduced far upstream of the headform on a specific streamline at a chosen radius from the axis. Since little of current interest occurs until the bubble reaches neutral equilibrium, we simply jump quasistatically forward to the position on that same streamline at

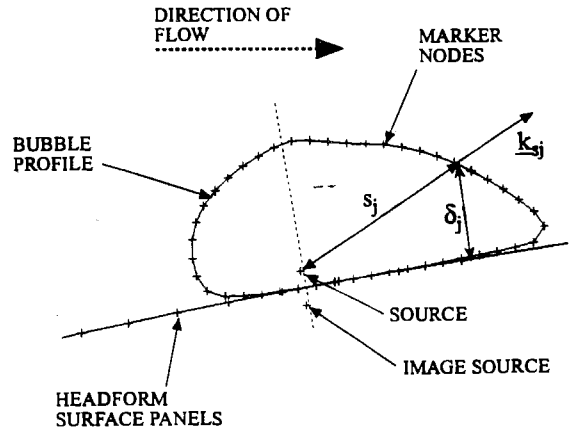

Fig. 3. Schematic showing the mid-plane profile of a bubble and the notation used in treating its evolution.

which the nucleus first becomes unstable (Blake 1948) and will then begin to grow explosively. This position is located in the low pressure region downstream of the point where $p = p_v$ or $C_p = -\sigma$.

The surface of the bubble is a material surface within the flow and its evolution is tracked in the following way (see figure 3). The mid-plane profile is defined at each time step by N_b equidistant marker nodes ($N_b = 45$ in the current calculations). The fluid velocity at each of these marker nodes is calculated from the solution of equation 3 and the profile at the next time step is obtained using displacements which are the fluid velocities multiplied by the time increment. The rest of the three-dimensional geometry of the bubble can be tracked in the same way. It follows that the kinematic condition on the bubble surface is quite accurately satisfied.

Now for the dynamic condition on the surface of the bubble. At each time step the liquid pressure on the exterior of the bubble surface can be calculated from the solution of equation 3 using the unsteady Bernoulli equation. We denote this by a coefficient of pressure, C_{plj}, $j = 1$ to N_b, for each of the marker nodes. Then the dynamic condition requires that this be equal to a pressure calculated knowing the surface tension, S, the vapor pressure and the partial pressure of air inside the bubble; this leads to terms which are very similar to those of the Rayleigh-Plesset equation for spherical bubbles and to a pressure coefficient, C_{pbj}, $j = 1$ to N_b, for each marker node given by

$$C_{pbj} = -\sigma + \left\{\sigma + \frac{4D}{R_0 We}\right\}\left\{\frac{V_0}{V}\right\}^k - \frac{4D}{\mathcal{R}_j We} + \frac{4D}{URe}\left\{\frac{\partial v_{nj}}{\partial n_j}\right\} \tag{4}$$

where $We = \rho U^2 D/S$, $Re = UD/\nu$, ν is the kinematic viscosity of the liquid,

V and V_0 are the current and initial volumes of the bubble, k is the polytropic constant for the air (1.4 is used in the present calculation) and $\mathcal{R}_j$, v_{nj} and n_j are respectively the radius of curvature of the bubble surface, the velocity normal to the surface and the surface normal at the marker node j. The dynamic surface condition at each marker node is therefore $C_{plj} = C_{pbj}$.

The program chooses both the strength, q, of the source and its location, (r_q, x_q), so as to minimize three integral properties involving the residuals $|C_{plj} - C_{pbj}|$. Thus the dynamic conditions are only satisfied in an approximate, averaged sense. It is clearly possible for the method to be extended and improved by the introduction of some other source variables such as would be created by the addition of higher order singularities. A corresponding number of other, higher order moments of $|C_{plj} - C_{pbj}|$ could then be minimized. In this paper we demonstrate that the three variables involved in using a simple source provide remarkably accurate information on the bubble shape dynamics.

In the current calculations an iterative procedure is used at each time step to determine the optimal values of q, r_q and x_q. Assuming a particular source location, a new value of q and a displacement vector, $\underline{d}$, of the location of the source are computed using:

$$q = \sum_{j=1}^{N_b} \delta_j q_j \Big/ \sum_{j=1}^{N_b} \delta_j \quad ; \quad \underline{d} = \sum_{j=1}^{N_b} \left\{ \delta_j \underline{k}_{sj} (q_j - q) \frac{\Delta C_{plj}}{\Delta q} \Big/ \frac{\Delta C_{plj}}{\Delta s_j} \right\} \Big/ \sum_{j=1}^{N_b} \delta_j \qquad (5)$$

where q_j is the source strength which would exactly satisfy the dynamic condition at the jth marker node, δ_j is the normal distance of the marker node from the headform surface, s_j is a coordinate along a line from the source to the jth node ($\underline{k}_{sj}$ is a unit vector in the same direction) and $\Delta C_{plj}/\Delta q$ and $\Delta C_{plj}/\Delta s_j$ are derivatives of C_{plj} with respect to the source strength and with respect to displacement of the source in the direction of s_j. The source is then displaced by $\underline{d}$ and the calculation repeated; usually three iterations were sufficient for convergence. Clearly, weighted summations could be chosen which would be different from those of equations 5 but tests showed that the above choice was reasonably effective.

This summarizes the basic elements of the computational method. A few additional features should be mentioned in passing. (i) As with many free surface problems, there is an inherent numerical instability which sometimes develops in which spatially alternating errors accumulate at the locations of the surface marker nodes. These alternating deformations had to be artificially damped. (ii) Tests showed that the modifications to the ring panel intensities caused by the presence of the bubble were very small and that the bubble dynamics were virtually unchanged when the q terms in equation 3 were omitted. This leads to major computational savings since the values of μ_i need only be determined once at the beginning of the computation. (iii) We have not attempted a complete review of all the approximations and error evaluations in this brief account. For example, a more accurate approach might involve dividing the ring panels into circumferential elements having different intensities rather than the circumferentially uniform

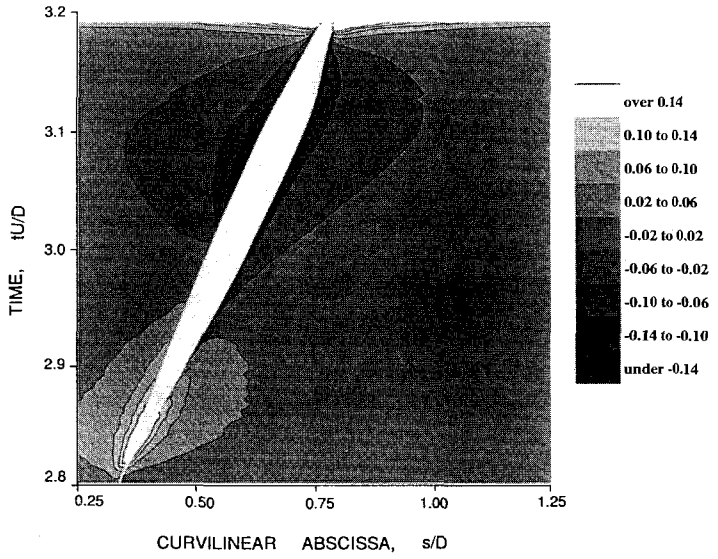

Fig. 4. Evolution of the increment in the pressure coefficient on a surface 1/100th of a headform diameter into the flow from the headform surface. The white object is the contour occupied by the bubble. The cavitation nnmber is 0.45.

intensity currently assumed. It transpires that the computational expense of such a refinement is not merited by the marginal improvement in accuracy. These and other error evaluations are detailed in Kuhn de Chizelle (1993).

Finally we emphasize that the basic three parameter version of the algorithm described above can only be expected to model the simpler features of the bubble geometry and not the complex features associated with a well-developed reentrant jet. This would require the addition of several more source parameters, an improvement that would be relatively straightforward.

3 Results

Information on how the perturbations to the flow change with time can be presented in the form shown in figure 4 which illustrates the evolution of the incremental coefficient of pressure caused by the bubble. The figure plots the incremental pressure coefficient on a surface which is parallel to the headform surface a specific distance into the flow (in this case 1/100th of a headform diameter). Note the positive incremental pressures surrounding the bubble as it grows and the negative incremental pressures as it collapses. The final stage of collapse is characterized by a large positive incremental pressure corresponding to the collapse noise spike. For much more information see Kuhn de Chizelle (1993). Such data allow evaluation of the potential for bubble/bubble interactions in more developed cavity flows and of the unsteady pressure distribution acting on the boundary layer.

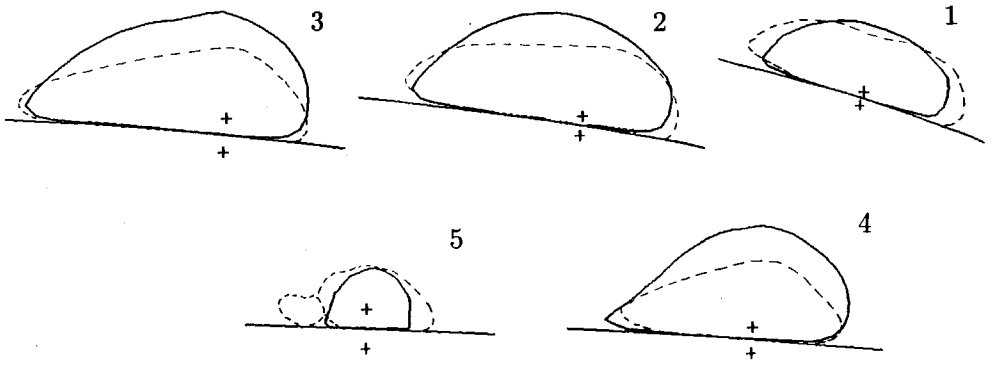

Fig. 5. Comparison between the experimentally observed profiles of the bubbles in Fig. 2 (dashed lines) and the profiles calculated by the three parameter version of the current algorithm (solid lines). The locations of the source and the image source are shown by the crosses.

4 Comparison with experiments

In figure 5 the experimental bubble profiles of figure 2 are compared with the profiles computed by the three parameter version of the current program at the same five moments in time (labelled 1 to 5) during the bubble evolution. It can be seen that the overall size of the bubbles are in good agreement with the observations and that there is qualitative agreement in the general shape of the bubble as well as the way it changes with time. Clearly the program reproduces the spherical cap shapes which are separated from the headform by a thin liquid layer. During the growth phase we note a minor depression in the top of the cap which is reminiscent of the dimples on the top of the bubbles observed by Kuhn de Chizelle *et al.* (1992) but not as pronounced. Later the bubble assumes the wedge-like shape similar to the experiments. The largest discrepancy is that the computed bubbles are not as elongated as those observed, particularly at the higher cavitation numbers. The three parameter version of the present algorithm may not be able to handle such large departures from sphericity.

The overall dimensions can also be compared with those measured by Kuhn de Chizelle *et al.* (1992) for bubbles on Schiebe headforms of different size. Figure 6 presents a comparison of the base radii of the observed and calculated bubbles as a function of the cavitation number. Note that in this figure the dimensions of the bubbles on the smallest headform could not be measured very accurately and therefore the data with the dotted lines should be regarded as much less reliable. The agreement with most of the data is quite satisfactory and shows a significant deviation from the radius of a spherical, Rayleigh-Plesset bubble calculated using the surface pressure distribution. The sphericity of the bubbles defined as the

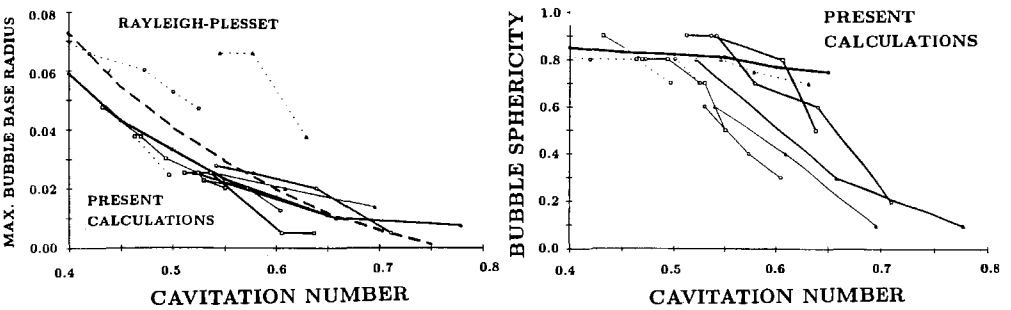

Fig. 6. The maximum radius of the base of the cavitation bubbles (normalized by D) and their sphericity as functions of the cavitation number, σ. Data from Kuhn de Chizelle *et al.* (1992) for three headform diameters (50.8 cm = thick solid line, 25.4 cm = thin solid line, 5.08 cm = dotted line) at three different tunnel velocities (9 m/s = $\triangle$, 11.5 m/s = o, 15 m/s = $\square$). The present calculations are shown by the solid line (with •). The results of a Rayleigh-Plesset calculation are also shown.

ratio of their maximum thickness normal to the headform surface divided by the maximum base radius is also shown in figure 6. Here again there is good agreement between the observations and the calculations but only for the lower cavitation numbers where the sphericity is large. As previously discussed, the experimental bubbles at the larger cavitation numbers are significantly flatter.

5 Conclusions

This paper presents a method for calculating the interaction between a travelling cavitation bubble and an irrotational flow field. Conventional boundary integral methods for the basic steady flow past a solid body are supplemented by a procedure which simulates a travelling cavitation bubble. This bubble interacts with the body and is deformed by the large pressure gradients in the vicinity of the minimum pressure point on the body surface. It is demonstrated that a simple model for the bubble consisting of a source/sink of varying intensity and location, when combined with an identical image source, provides a surprisingly accurate representation for this complicated unsteady flow. The method is applied to travelling cavitation bubbles in the flow around an axisymmetric headform (a Schiebe body) and the results are compared with the experimental observations of Ceccio and Brennen (1991). The calculated bubble shapes are very similar to those observed experimentally and the calculations permit an understanding of the way in which the bubble alters the flow. Since the method is quite modest in its computational requirements, further studies may include the use of the model to study the interactions between bubbles when several are introduced to the flow. The present

solutions also provide a necessary prerequisite for the study of the unsteady viscous interactions between the bubble and the boundary layer, a study which is clearly required in order to understand some of the other interactions observed experimentally by Ceccio and Brennen (1991) and Kuhn de Chizelle *et al.* (1992).

6 Acknowledgments

The authors would like to thank Allan Acosta for his continuing help and encouragement and Steven Ceccio for his valuable assistance. We are grateful for the support provided by the Office of Naval Research under contract N00014-91-J-1295.

References

Benjamin, T. B. and Ellis, A. T.: 1988, *Phil. Trans. Roy. Soc., London, Ser. A.*, **Vol. no. 260**, pp. 221–240.

Blake, F.G.: 1949, *Acoustics Res. Lab., Harvard Univ., Tech. Memo. No. 12.*

Blake, W. K., Wolpert, M. J. and Geib, F. E.: 1977, *J. Fluid Mech.*, **Vol. no. 80**, pp. 617–640.

Briancon-Marjollet, L. and Franc, J. M.: 1990, *J. Fluid Mech.*, **Vol. no. 218**, pp. 355–376.

Ceccio, S. L. and Brennen, C. E.: 1991, *J. Fluid Mech.*, **Vol. no. 233**, pp. 633–660.

Chahine, G.: 1992, *Personal communication.*

Ellis, A.T.: 1952, *Calif. Inst. of Tech. Hydr. Lab. Rep., 21-12.*

Fujikawa, S. and Akamatsu, T.: 1980, *J. Fluid Mech.*, **Vol.no. 97**, pp. 481–512.

Gilmore, F. R.: 1952, *Calif. Inst. of Tech. Hydrodyn. Lab. Rep. No. 26-4.*

Hickling, R. and Plesset, M. S.: 1964, *Phys. Fluids*, **Vol. no. 7**, pp. 7–14.

Kellogg, O.D.: 1953, *Foundations of Potential Theory.* Dover.

Kimoto, H.: 1987, *Int. ASME Symp. on Cavitation Res. Facilities and Techniques*, **Vol. no. FED 57**, pp. 217–224.

Knapp, R.T. and Hollander, A.: 1948, *Trans. ASME*, **Vol. no. 70**, p. 419.

Kuhn de Chizelle, Y., Ceccio, S.L., Brennen, C.E. and Gowing, S.: 1992, *Proc. 3rd I.Mech.E. Int. Conf. on Cavitation, Cambridge, England*, pp. 165–170.

Kuhn de Chizelle, Y., Ceccio, S.L., Brennen, C.E. and Shen, Y.: 1992, *Proc. 19th Symp. on Naval Hydrodynamics, Seoul, Korea*, pp. 72–84.

Kuhn de Chizelle, Y.: 1993, *Ph.D. Thesis, Calif. Inst. of Tech.*

Kumar, S. and Brennen, C.E.: 1993, *J. Fluid Mech.*, **Vol. no. 255**, pp. 541–564.

Lauterborn, W. and Bolle, H.: 1975, *J. Fluid Mech.*, **Vol. no. 72**, pp. 391–399.

Naude, C. F. and Ellis, A. T.: 1961, *ASME J. Basic Eng.*, **Vol. no. 83**, pp. 648–656.

Parkin, B.R.: 1952, *Ph.D. Thesis, Calif. Inst. of Tech.*

Shima, A., Takayama, K., Tomita, Y. and Miura, N.: 1981, *Acustica*, **Vol. no. 48**, pp. 293–301.

Shima, A., Takayama, K., Tomita, Y. and Ohsawa, N.: 1983, *AIAA J.*, **Vol. no. 21**, pp. 55–69.

van der Meulen, J. H. J. and van Renesse, R. L.: 1989, *Proc. 17th Symp. on Naval Hydrodynamics, The Hague*, pp. 195–217.